Proceedings of GPPS Forum 18
Global Power and Propulsion Society
Montreal, 7th-9th May 2018
www.gpps.global

GPPS-2018-0004

STEADY AND UNSTEADY FLOW PHENOMENA IN AN ENGINE INTAKE RESEARCH DUCT WITH AND WITHOUT PASSIVE FLOW CONTROL

Rudolf P. M. Rademakers
Institute of Jet Propulsion, Bundeswehr University Munich
ruud.rademakers@unibw.de
Neubiberg, Germany

Marcel Stößel
Wehrtechnische Dienststelle für Luftfahrzeuge und Luftfahrtgerät der Bundeswehr
Manching, Germany

Reinhard Niehuis
Institute of Jet Propulsion, Bundeswehr University Munich
Neubiberg, Germany

ABSTRACT

The full integration of the propulsion system is an important requirement for military aircraft in order to reduce their radar signature and to increase overall aerodynamic performance. This leads to short and highly bent engine intake ducts, which typically provoke severe flow distortions close to the compressor system. Especially in compact systems the flow within both the intake duct and the compressor interacts.

In the last decades the intake duct and the compressor system have predominantly been designed separately. Nevertheless, the aerodynamic intake-compressor interactions have to be considered during the design of highly compact and thus aerodynamically coupled propulsion systems. The Institute of Jet Propulsion at the Bundeswehr University Munich hence developed a military engine intake duct specifically for research purposes. The research duct can be tested in both a remote- and close-coupled configuration with the Larzac 04 turbofan engine. Different types of adapters integrated within the duct's structure enable extensive wall pressure measurements and moreover a flexible integration of flow control devices.

This paper evaluates the commissioning of the research duct in several configurations. It is focused on, first, the initial design of a passive flow control device, which serves as base design for further studies on flow control in the research duct. Second, time-resolved static wall pressure measurements at various positions reveal the unsteady character of the flow within the range of $0.21 < St < 0.26$, which is most probably related to a mass flow fluctuation within the duct.

INTRODUCTION

Future military aircraft have to fulfil high expectations in terms of propulsive performance and minimum radar signature, which makes propulsion system integration into the fuselage indispensable. The main benefits of a compact and integrated propulsion system are a shorter overall aircraft length (and thus also a weight saving), a reduction of aerodynamic drag, and enhanced stealth characteristics due to decreased visibility of rotating compressor components.

A combined pressure-swirl distortion is inevitably provoked in serpentine ducts. The distorted flow cannot homogenize and will strongly interact with the compressor flow. Hence, flow distortion influences the stability and performance of the propulsion system.

The Institute of Jet Propulsion designed and developed the so-called military engine intake research duct (MEIRD) to enable diverse experimental investigations on a highly bent intake duct coupled with a turbofan engine. The results obtained during the commissioning of the setup are presented in this paper to show the research opportunities of this experimental setup. A main focus was put on the design of an initial passive flow control (PFC) device and determining the unsteady character of the ducted flow. In the following these two topics are hence briefly introduced.

Passive flow control in s-ducts

Vortex generators (VGs) are used for PFC in different fields of mechanical engineering. Lin (2002) presents a general review on flow control by using VGs for different kinds of applications.

PFC is a relatively simple and cost-efficient method for flow optimization in a bent engine intake duct, especially because such devices can be developed as retrofitting solution. Bauermeister (1968) presented an early and successful application of VGs to improve the flow in the s-duct intake of the Boeing 727 center engine.

The application of VGs in s-duct engine intakes has quite often been investigated in the last decades. A general conclusion from earlier presented publications is that the VG design is very application dependent and it is nearly

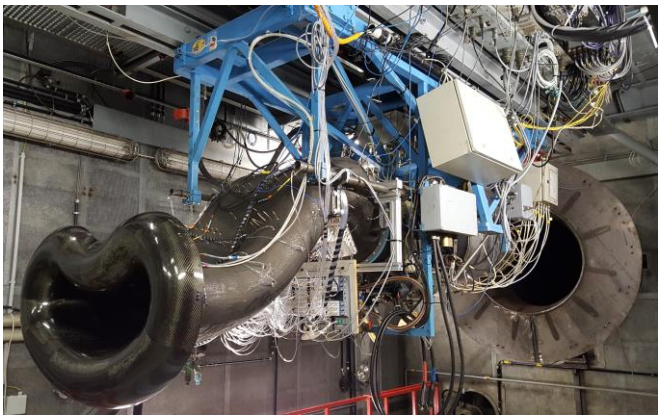

Figure 1 Military Engine Intake Research Duct (MEIRD) installed with the Larzac 04 test vehicle at the Engine Test Facility (ETF)

impossible to establish a general guideline for this kind of flow control in s-ducts. On the whole, publications by Reichert and Wendt (1996), Hamstra et al. (2000), Anabtawi et al. (1999), and Jirásek (2006) have inspired for the PFC design presented in this publication.

The effectiveness of PFC in s-ducts is commonly evaluated by the improvement of the flow condition at the duct outlet plane (DOP). Investigations on flow control in the MEIRD, however, enable a direct analysis on the improvement of engine performance and stability by the flow control device.

Flow unsteadiness in s-ducts

Since the development of the F-111 aircraft in the 1960s it is known that a dynamic total pressure inflow distortion can influence the engine operability, Society of Automotive Engineers (2016). Unsteady flow phenomena within engine intake ducts have not often been investigated in the open literature yet. Nevertheless, complex unsteady flow phenomena occur in s-ducts, which motivates respective measurements within the MEIRD. The Strouhal number

$$St = \frac{f \cdot l}{U} \quad (1)$$

is typically used to describe oscillating flow mechanisms. In this equation f is the frequency of the flow fluctuation, l is a chosen characteristic length, and U is the bulk flow velocity. The duct entry plane diameter is often chosen as characteristic length.

Garnier (2015) conducted experiments on an s-duct with an averaged Mach number at a measurement plane downstream of the duct between 0.2 and 0.4. The flow condition was within the range of $0.75 \cdot 10^6 < Re_d < 1.5 \cdot 10^6$, where the Reynolds number is based on the duct entry plane diameter. Dominant total pressure fluctuations at the measurement plane within the range of $0.25 < St < 0.625$ were detected at both Mach number levels.

Stereoscopic particle image velocimetry measurements by Gil-Pietro et al. (2017) reveal that the measured time-resolved flow patterns significantly differ from the mean flow

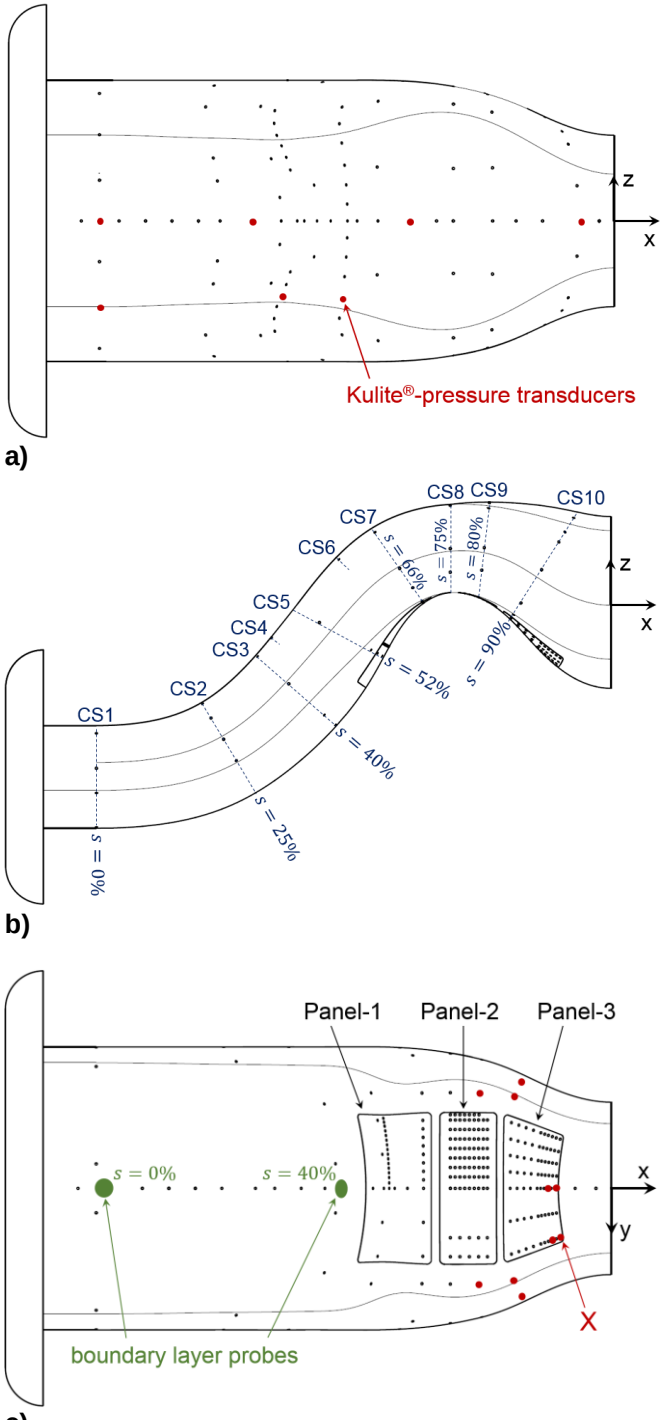

Figure 2 Schematic representation of the MEIRD with important measurement positions: a) top side b) side view c) bottom side

pattern at the outlet plane of two s-duct configurations. A vertical mode of the unsteady flow is identified, which is related with a shear layer instability. Furthermore, a switching mode is associated with a modulation of the secondary flow within the duct. Gil-Pietro et al. (2018) conducted further investigations on the high-offset duct at $Re_d = 0.71 \cdot 10^6$, where the Reynolds number is based on the duct entry plane diameter. The variation of the time-resolved evaluated

distortion descriptors is within the range of $0.53 < St < 1.09$.

EXPERIMENTAL SETUP

Larzac 04 C5 turbofan engine

The Institute of Jet Propulsion operates several types of military aircraft engines at the engine test facility (ETF) for both educational as well as research purposes. The institute has great experiences with the Larzac 04C5 turbofan engine, which was chosen for the investigations with the MEIRD (cf. Fig 1). The Larzac 04 engine is equipped with extensive instrumentation in its low pressure compressor and the setup can easily be adapted, which makes it an ideal test vehicle for current investigations.

Military Engine Intake Research Duct

The geometry of the MEIRD is shown in Fig. 2. The surface length s in Fig. 2 describes the relative position along the flow path within the xz-symmetry plane. The geometry was designed by Rademakers et al. (2016b) to be similar to an intake duct of a modern single engine military aircraft and hence provokes an application typical combined pressure-swirl distortion. On the other hand, it was taken into account that the duct needs to be applicable for various experimental investigations. The most important design features for the latter purpose are summarized in the following:

The cross section (CS) at $s = 0\%$ is named duct inlet plane (DIP). Upstream of the DIP a lip with a bellmouth-shape ensures a best possible homogeneous inflow condition. It is noted that the duct was built for research on duct internal flow phenomena only.

The duct features 363 integrated adapters for static wall pressure measurements. Generally, a brass sensor consisting of a drill hole ($d_{sensor} = 1mm$) with a plug-in sleeve on the outer side of the duct is installed. A tube is used to connect these sensors with a pressure transducer. Alternatively, a sensor with an integrated Kulite®-pressure transducer can be installed for local time-resolved wall pressure measurements to assess the unsteady behavior of the ducted flow. The respective positions where Kulite®-transducers were installed are indicated with red dots in Fig. 2.

A large scale flow separation occurs at the bottom side of the duct. It was decided to integrate three replaceable panels within this region (cf. Fig. 2c). The first panel (Panel-1) is integrated upstream of the flow separation. Panel-2 and Panel-3 are located within the region of the flow separation onset and the region of the flow reattachment, respectively. The three panels enhance the possibilities for detailed flow measurements and the installation of devices for flow stabilization.

Two probe mountings were integrated at the bottom side of the wall at the symmetry plane. These mountings were mainly used for the installation of boundary layer probes. The first mounting is positioned at $s = 0\%$ and the second one shortly upstream Panel-1 at $s = 40\%$.

TEST CASES

During the commissioning of the MEIRD it was focused on gaining an overall understanding of steady and unsteady flow phenomena within the research duct with and without passive flow control. The chapter *Results* is divided in three sections: *Reference configuration*, *Passive flow control*, and *Unsteady flow*, which are briefly introduced in the following.

The duct was tested in its reference configuration (i.e. without a flow control device) to, first, check the operating range of the Larzac 04 engine with the research duct installed. Secondly, the flow separation onset position and the boundary layer thickness upstream of the flow separation was measured since these two parameters are of main importance for the design of a suitable PFC device.

The PFC device was then designed based on knowledge gathered from the open literature. The obtained results with this device are presented in this paper.

In the third section, the results from the time-resolved wall pressure measurements with Kulite®-pressure transducers are summarized to assess the unsteady behavior of the flow inside the duct.

The experimental data presented in this paper is moreover of great importance for the validation of CFD simulations on

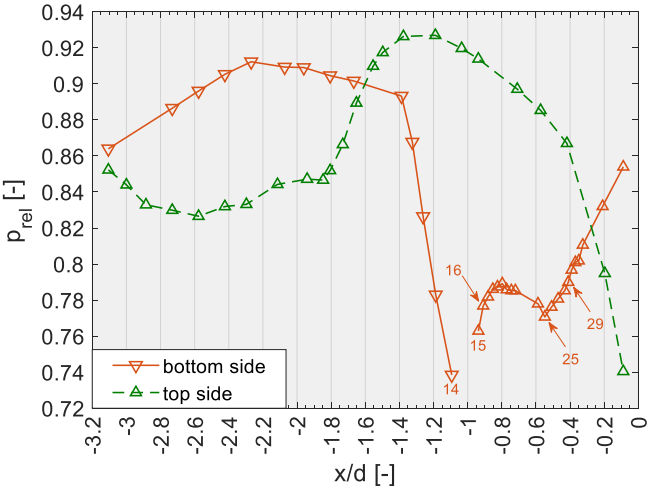

Figure 3 Static wall pressure within the xz-symmetry plane for $n_{red} \approx 95\%$

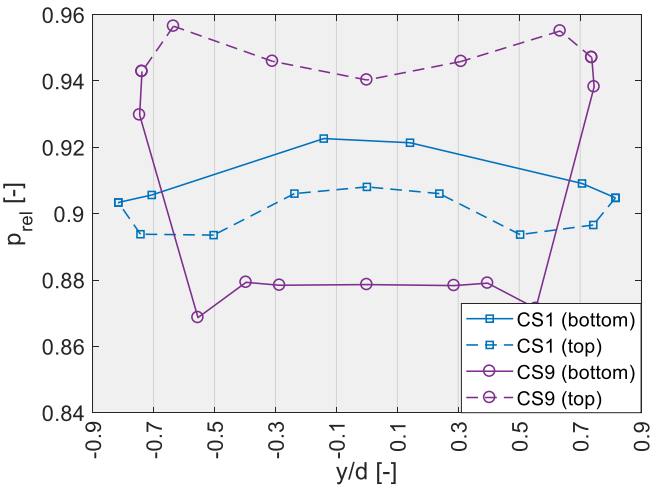

Figure 4 Static wall pressure within cross section 1 and 9 for $n_{red} \approx 76\%$

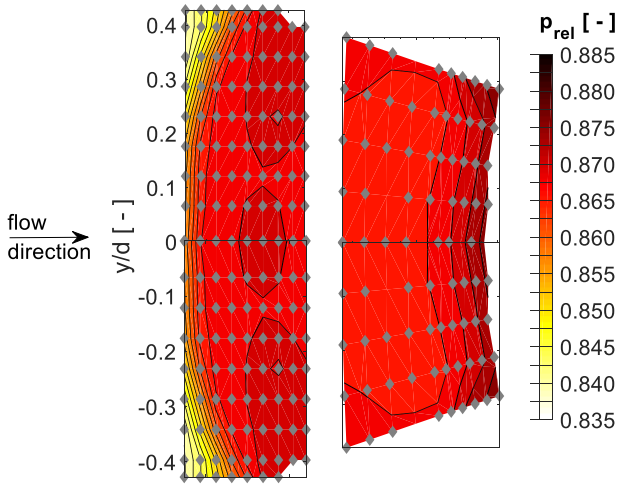

Figure 5 Static wall pressure within the region of flow separation measured with pressure taps in Panel-2 and Panel-3 for $n_{red} = 76\%$

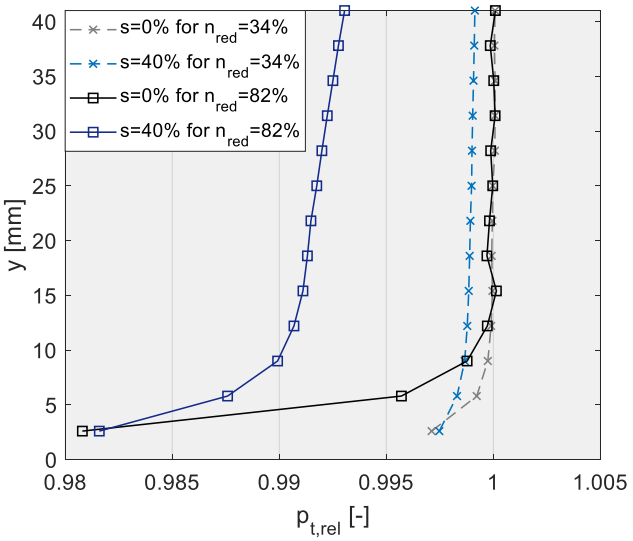

Figure 6 Total pressure within the boundary layer at the positions $s = 0\%$ and $s = 40\%$ for the thrust settings $n_{red} = 34\%$ and $n_{red} = 82\%$

the reference configuration by Haug et al. (2018) and the setup with the PFC conducted by Kächele et al. (2018). For the interested reader it is noted that another testing setup with a bent duct coupled with the MexJET test vehicle (Rademakers et al., 2018) is available at the ETF for experimental investigations in the same field of research.

DEFINITIONS

The measured static and total pressure values are presented in this paper relative to a reference pressure, which is measured at a fixed position within the test cell. It is noted that this reference pressure drops for increasing thrust settings of the engine, since the flow through the test cell generates a depression.

RESULTS AND DISCUSSION

Reference configuration

The static wall pressure within the xz-symmetry plane is shown in Fig. 3 for the engine operating point (EOP) $n_{red} = 95\%$, which is the maximum thrust setting for the Larzac 04 during operation at the ETF.

All data points are connected in a linear manner, except the data points 14 and 15. This has the following reason: a strong flow acceleration on the duct's bottom side, caused by the first s-bend, is visible between $-1.39 < x/d < -1.09$. The minimal wall pressure value is, however, expected to occur downstream of data point 14 (i.e. $x/d = -1.09$). A wall pressure tap could not be integrated, since the mounting for Panel-1 and Panel-2 is integrated within the duct's structure here. The calculated isentropic Mach number is 0.67 for the lowest measured wall pressure ($p_{rel} = 0.739$) for $n_{red} = 95\%$. The flow is expected to remain subsonic also in the case of a potential further acceleration downstream data point 14.

Then, the flow decelerates and becomes prone to flow separation due to the second s-bend within the duct. Normally, a pressure plateau reveals the flow separation within static wall pressure data. A distinct plateau is not visible in Fig. 3, nevertheless, a flow separation occurs roughly between data point 16 and 29 as it is shown by further wall pressure measurements presented later on.

The static wall pressure starts increasing downstream of point 25 and hence, it is expected that the flow is fully reattached at the DOP. This is important because flow measurements would be difficult in the case flow separation would extent until the DOP. The flow condition downstream of DOP is not measured yet, however, this is planned with a traversable rake featuring both five-hole probes and Kiel-probes during future testing campaigns. Since the Larzac 04 test vehicle could be operated within its entire operating range $idle < n_{red} < 95\%$ it is shown that the provoked distorted compressor inflow is within the engine limits as determined by Rademakers et al. (2016a). Tests with the research duct at the ETF are within the range of $0.9 \cdot 10^6 < Re_d < 2.9 \cdot 10^6$, where the hydraulic diameter of the DIP is used as reference length.

Static wall pressure is also measured along the flow path within ten cross sections (cf. Fig. 2). The static wall pressure within CS1 varies along its circumference (see Fig. 4). This is explained by the angled inflow of the MEIRD during operation at the ETF due to a complex macro-aerodynamic flow condition within the test cell. The angled inflow leads to a non-uniform total and static pressure at the DIP, cf. Rademakers et al. (2018). The wall pressure in CS9 shows a clear pressure plateau, which indicates a severe flow separation between $-0.397 < y/d < 0.397$.

The flow separation is best visible in Fig. 5, where static wall pressure measurements within Panel-2 and Panel-3 are shown. The wall pressure was measured with 120 wall pressure taps within one half of both panels. These data are mirrored in Fig. 5 with respect to the x-axis for the sake of clarity. This is valid since the static wall pressure is symmetric with respect to the xz-symmetry plane within the entire duct

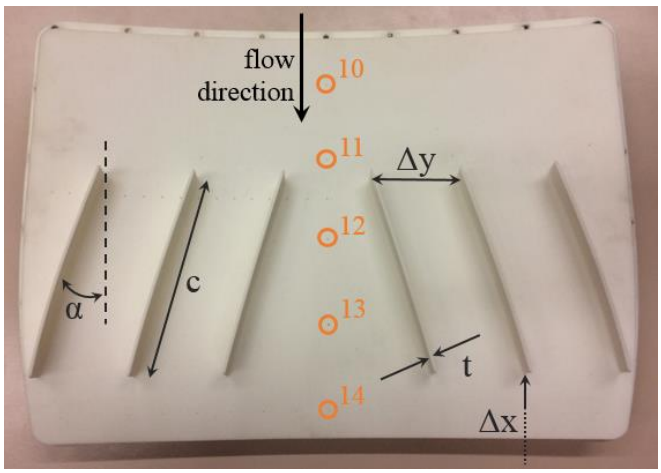

Figure 7 Panel-1 equipped with six vortex generators (CFG00) for passive flow control in the research duct

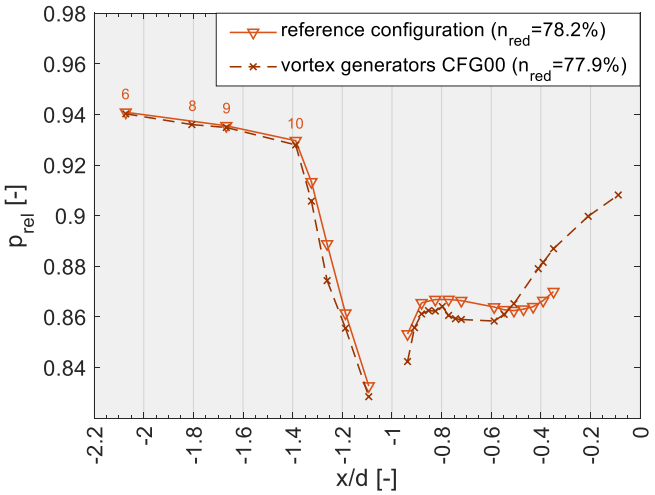

Figure 8 Comparison of the static wall pressure at the duct's bottom within the xz-symmetry plane for the configurations with and without passive flow control for $n_{red} = 78\%$

number of VGs	n	6
height	h/δ	1.33
chord	c/h	7
distance to flow separation onset	$\Delta x/h$	12
lateral distance between VGs	$\Delta y/h$	3
angle of attack	α	16°
vane thickness	t	$2mm$

Table 1 Geometry of the vortex generators on the CFG00 PFC device

as it is exemplarily shown for CS1 and 9 in Fig. 4. The original data is measured within the range of $-0.427 < y/d < 0$ solely. Between $0 < y/d < 0.427$ wall pressure was measured with a much lower resolution (see Fig. 2c). The highly negative pressure gradients close to the front end of Panel-2 and the rear end of Panel-3 indicate the position of the flow separation onset and the flow reattachment, respectively. The extension of the separation is well captured in the reference configuration and hence, the flow separation can also be visualized in all further test cases with flow control devices, where the separation extent in principle should be reduced.

The boundary layer profile is visualized at the positions $s = 0\%$ and 40% in Fig. 6 by means of the total pressure relative to a reference pressure within the test cell ($p_{t,rel}$) in a radial distance from the wall between $2.6mm < y < 41mm$. Several interesting observations from these data can be drawn: the boundary layer thickness at $s = 0\%$ increases from $\delta \approx 10mm$ up to $15mm$ over the engine operating range. At this position (i.e. the DIP) δ can be estimated with e.g. the $0.99 \cdot \delta$-criterion. A similar approximation for δ at $s = 40\%$ is not possible due to the variation of total pressure within this CS. Hence, it was chosen to define δ as radial position y from which the measured $p_{t,rel}$ increases linearly. In this case, δ is comparable to $s = 0\%$, i.e. $\delta \approx 10mm$ ($n_{red} = idle$) and $\delta \approx 15mm$ (full thrust). Furthermore, a significant pressure loss occurs between $0\% < s < 40\%$, especially for higher thrust settings. This can partly be explained by the complex secondary flow generating total pressure losses within the duct. Nevertheless, the boundary layer probe installed at $s = 0\%$ might also be responsible for a part of total pressure loss, which becomes apparent at $s = 40\%$.

Passive flow control

Panel-1 is located upstream of the region with flow separation and hence, designated for the integration of PFC devices. An initial configuration of VGs (CFG00) at the location of Panel-1 was designed based on knowledge from the open literature (see Ch. *Introduction*) to perform first experimental investigations on PFC within the MEIRD. Kächele et al. (2018) used the experimental data to validate a setup for CFD simulations, which is subsequently used to establish optimized VG configurations. These configurations will also be tested experimentally in the near future.

The selective laser sintering production method is used to manufacture the panels with VGs since this enables a quick, precise, and cost-efficient manufacturing. A polyamide is used as material because of its surface quality, sufficient mechanical resistance, and long-term stability. Panel-1 is installed in a region with a high duct core flow velocity and hence a very low local static wall pressure compared to the outer side of the duct. Significant loads occur due to this wall pressure difference and thus the outer side of the panel had to be reinforced with a sandwich-like structure, which can easily manufactured while using the sintering process. This reinforcement ensures a minimal deformation (i.e. less than $1mm$) of the panel due to wall pressure during engine operation. The predictable structural behavior of a sintered polyamide component enables realistic numerical structural finite element analyses, which proved the structural integrity of the panel during engine tests. Figure 7 shows the panel including VG CFG00. The main parameters of the VGs are listed in Tab. 1.

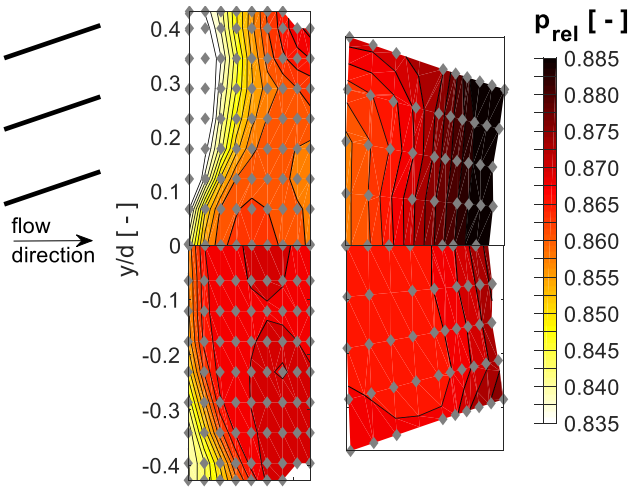

Figure 9 Comparison of the static wall pressure within the region of flow separation between the CFG00 (top) and the reference configuration (bottom) for $n_{red} = 76\%$

The static wall pressure within the xz-symmetry plane for both cases (i.e. with and w/o PFC) is compared in Fig. 8. The data points 6, 8, 9, and 10 are positioned in a significant distance upstream of the VGs and hence the local wall pressure matches for both experiments with similar thrust settings. The inner VGs represent sort of a diffuser for the flow, which is visible by a slightly lower wall pressure downstream of data point 10 for the VG case. The position of flow separation onset does not seem to be changed compared to the reference configuration, but the reattachment occurs earlier and the static wall pressure increases to higher values towards the DOP.

The static wall pressure data measured within Panel-2 and Panel-3 (see Fig. 9) give a better inside of the VGs influencing the flow. It is noted that Fig. 9 combines data from two separated engine runs. The data from the VG case are mirrored with respect to the x-axis. The VGs in the upper left corner are schematically shown, but not to scale.

The flow separation onset is nearly unchanged within the symmetry plane because of missing VGs in this plane at Panel-1. The induced vortices lift off near the trailing edge of the VGs and apparently do not expand quickly enough. A delay of the flow separation onset is visible further aside from the symmetry plane. The position of the flow reattachment is much earlier compared to the reference configuration and visible by strong positive wall pressure gradient within the middle of Panel-3. The effectiveness of CFG00 is now also apparent within the symmetry plane, since the reattachment occurs at a fairly constant position. The size of the separated area is reduced significantly. As mentioned earlier, a detailed measurement of the DOP is necessary for further analyses on the effects of VG CFG00 on intake performance.

Unsteady flow

Kulite®-pressure transducers were installed at 17 different positions, as shown in Fig. 2, within the research duct during engine runs. In general, data was measured with a

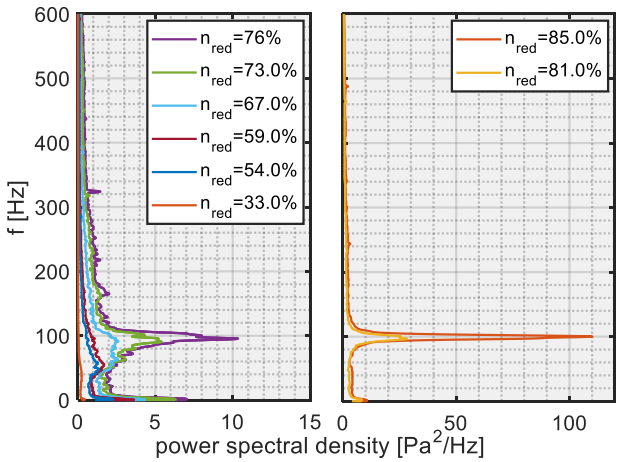

Figure 10 Power spectral density of the time-resolved wall pressure at position X for thrust settings within the range of $33\% < n_{red} < 85\%$

$20kHz$ sampling rate over a time period of $120s$ at various engine thrust settings within the range of $Idle < n_{red} < 85\%$. Figure 10 shows the power spectral density of the time-resolved static wall pressure data at the position X (cf. Fig. 2c). Distinct peaks are visible for highest investigated thrust settings in the range of $73\% < n_{red} < 85\%$. This dominant frequency does not vary significantly over this part of the operating range. The calculated Strouhal number varies between $St = 0.26$ for $n_{red} = 73\%$ and $St = 0.21$ for $n_{red} = 85\%$. The same observations are made with the measurement data of all other positions, however, they are most distinct at position X. It is expected that this global flow unsteadiness relates to a mass flow fluctuation within the duct. The previously described flow unsteadiness is reduced to a minimum for the test case including VG CFG00. For this case a slight increase of the power spectral density within the range of $0.21 < St < 0.26$ is still visible, however, without a distinct peak as for the case without passive flow control.

CONCLUSIONS

The paper presents the commissioning of an engine intake research duct coupled with the Larzac 04 turbofan engine at an engine test bed. The most important results can be summarized as follows:

1. The duct could be operated safely within the entire operating range of the Larzac 04 test vehicle at the ETF.
2. The design goals of the research duct are fully achieved: A severe flow separation is present within the expected region close enough to the DOP to provoke aerodynamic intake-compressor interactions. The flow is reattached at the DOP, which enables flow measurements with pressure probes. Two wall elements are positioned in this region and equipped with extensive wall pressure taps to visualize the separation.
3. The position of the flow separation onset and the boundary layer thickness δ upstream of the flow

separation onset was measured. With these data and knowledge from open literature, the initial design of a passive flow control device (CFG00) was established and tested.

4. The CFG00 PFC device clearly decreases the extent of the flow separation. The measurement data was used to validate CFD simulations and design improved types of flow control devices for experimental testing in the near future.
5. An unsteady character of the ducted flow was detected within the range of $0.21 < St < 0.26$, which is most probably related to a mass flow fluctuation of the ducted flow.

NOMENCLATURE

Symbols

d	$[mm]$	diameter
f	$[Hz]$	frequency
n_{red}	[%]	corrected relative LPC spool speed
p_{rel}	$[-]$	relative static wall pressure
$p_{t,rel}$	$[-]$	relative total pressure
Re	$[-]$	Reynolds number
s	[%]	relative position
St	$[-]$	Strouhal number
x,y,z	$[-]$	Cartesian coordinates
δ	$[mm]$	boundary layer thickness

Abbreviations

CFD	computational fluid dynamics
CFG	configuration
CS	cross section
DIP	duct inlet plane
DOP	duct outlet plane
ETF	engine test facility
EOP	engine operating point
MEIRD	military engine intake research duct
PFC	passive flow control
VG	vortex generator

REFERENCES

Anabtawi, A., Blackwelder, R., Lissaman, P., and Liebeck, R. (1999). An experimental investigation of boundary layer ingestion in a diffusing S-duct with and without passive flow control. In: Proceedings of the 37th Aerospace Sciences Meeting and Exhibit, January 1999, Reno, NV, USA. doi: 10.2514/6.1999-739

Bauermeister, W. K., Roseburg, C. M., and Ip, H. W. (1968). 727 airplane engine inlet development. In: Proceedings of the 4th Propulsion Joint Specialist Conference, June 1968, Cleveland, OH, USA. AIAA-68-595

Garnier, E. (2015). Flow Control by Pulsed Jet in a Curved S-Duct: A Spectral Analysis. AIAA Journal, 53(10), pp. 2813–2827. doi: 10.2514/1.J053422

Gil-Prieto, D., MacManus, D. G., Zachos, P. K., and Bautista, A. (2018). Assessment methods for unsteady flow distortion in aero-engine intakes. Aerospace Science and Technology, 72, pp. 292–304. doi: 10.1016/j.ast.2017.10.029

Gil-Prieto, D., MacManus, D. G., Zachos, P. K., Tanguy, G., and Menzies, K. R. (2017). Convoluted Intake Distortion Measurements Using Stereo Particle Image Velocimetry. AIAA Journal, 55(6), pp. 1878–1892. doi: 10.2514/6.2016-3560

Hamstra, J., Miller, D., Truax, P., Anderson, B., and Wendt, B. (2000). Active Inlet Flow Control Technology Demonstration. In: Proceedings of the 22nd Congress of the ICAS, August-September 2000, Harrogate, UK. ICAS 2000-6.11.2

Haug, J. P., Rademakers, R. P. M., Stößel, M., and Niehuis, R. (2018). Numerical Flow Field Analysis in a Highly Bent Intake Duct. In: Proceedings of the ASME Turbo Expo 2018, June 2018, Lillestrøm, Norway. GT2018-76633

Jirásek, A. (2006). Design of Vortex Generator Flow Control in Inlets. Journal of Aircraft, 43(6). doi: 10.2514/1.21364

Kächele, T., Rademakers, R. P. M., Stößel, M., and Niehuis, R. (2018). CFD based Optimization of Vortex Generator Flow Control in a Highly Bent Intake Geometry using Design of Experiments. In: Proceedings of the AIAA Aerospace Sciences Meeting 2018, January 2018, Kissimmee, FL, USA. AIAA-2018-0407

Lin (2002). Review of research on low-profile vortex generators to control boundary-layer separation. Progress in Aerospace Sciences, 38(4–5), pp. 389–420. doi: 10.1016/S0376-0421(02)00010-6

Rademakers, R. P. M., Bindl, S., and Niehuis, R. (2016a), Effects of Flow Distortions as They Occur in S-Duct Inlets on the Performance and Stability of a Jet Engine. ASME J. Eng. Gas Turbines Power, 138(2). doi: 10.1115/1.4031305

Rademakers, R. P. M., Haug, J. P., Niehuis, R., and Stößel, M. (2016b). Design and Development of a Military Engine Inlet Research Duct. In: Proceedings of the 30th Congress of the ICAS, September 2016, Daejeon, Korea. ICAS2016-0623

Rademakers, R. P. M., Probst, H., Schneider, T., and Niehuis, R. (2018). Experimental Investigations on a Bent Engine Inlet Duct Coupled with a Turbofan Engine. In: Proceedings of the AIAA Aerospace Sciences Meeting 2018, January 2018, Kissimmee, FL, USA. AIAA-2018-1353

Reichert, B. and Wendt, B. (1996). Improving curved subsonic diffuser performance with vortex generators. AIAA Journal, 34(1). doi: 10.2514/3.13022

Society of Automotive Engineers (2016). Inlet/Engine Compatibility – From Model to Full Scale Development. SAE Aerospace Information Report 5687, Rev. A